



Acid is a potential interferent in fluorescent sensing of chemical warfare agent vapors

Shengqiang Fan¹, Genevieve H. Dennison², Nicholas FitzGerald², Paul L. Burn¹ [✉], Ian R. Gentle¹ & Paul E. Shaw¹ [✉]

A common feature of fluorescent sensing materials for detecting chemical warfare agents (CWAs) and simulants is the presence of nitrogen-based groups designed to nucleophilically displace a phosphorus atom substituent, with the reaction causing a measurable fluorescence change. However, such groups are also basic and so sensitive to acid. In this study we show it is critical to disentangle the response of a candidate sensing material to acid and CWA simulant. We report that pyridyl-containing sensing materials designed to react with a CWA gave a strong and rapid increase in fluorescence when exposed to Sarin, which is known to contain hydrofluoric acid. However, when tested against acid-free diethylchlorophosphate and di-*iso*-propylfluorophosphate, simulants typically used for evaluating novel G-series CWA sensors, there was no change in the fluorescence. In contrast, simulants that had been stored or tested under a standard laboratory conditions all led to strong changes in fluorescence, due to acid impurities. Thus the results provide strong evidence that care needs to be taken when interpreting the results of fluorescence-based solid-state sensing studies of G-series CWAs and their simulants. There are also implications for the application of these pyridyl-based fluorescence and other nucleophilic/basic sensing systems to real-world CWA detection.

¹Centre for Organic Photonics & Electronics, School of Chemistry and Molecular Biosciences, The University of Queensland, Brisbane, QLD, Australia. ²Land Division, Defence Science & Technology Group, Fishermans Bend, VIC, Australia. ✉email: p.burn2@uq.edu.au; p.shaw3@uq.edu.au

Highly toxic organophosphorus (OP) compounds have been developed as chemical warfare agents that target the nervous system¹. Inhalation of the nerve agent or sorption through the skin or eyes leads to acetylcholinesterase (AChE) inhibition and an increase in acetylcholine², which results in muscle overstimulation and potentially death. Nerve agents are conventionally divided into two main classes, the G- and V-series. Given the toxicity of nerve agents and reports of their use in both military and civilian settings, there is a drive to develop technologies that the military, first responders (national security), healthcare and environmental monitoring agencies can deploy in the field to confirm their presence. While methods such as gas chromatography-mass spectroscopy (GC-MS)³, enzyme-based biosensors^{4–6}, chemiresistors^{7–9}, and surface acoustic wave (SAW) sensors can be used for the detection of nerve agents^{10,11}, they can suffer from a range of issues including being slow, nonselective, expensive, or simply too cumbersome for field use. Building on the success of fluorescence-based detection of explosives^{12–15} there has been an increasing number of reports of using a change in a fluorescence signal for the sensing of nerve agents^{16–18}. Given the electrophilic nature of the phosphorus atom in nerve agents, it is not surprising that the most commonly used strategy has been to develop a nucleophilic organic sensing compound that can react with the nerve agent^{19–51}, although organometallic sensing materials have also been studied^{52–55}. The design logic is based on the nucleophile of the sensing compound displacing one of the groups attached to the phosphorus atom, and generating a product whose fluorescence is different in either intensity or wavelength to that of the original sensing material. Nitrogen and oxygen-based nucleophiles have been most commonly used for organic sensing compounds designed to detect nerve agents^{19–51}, with the pyridyl moiety (or its fused ring analogs quinoline and quinoxaline) featuring as the nucleophilic group in the majority of the sensing materials^{19–30,42–46}. However, a key issue that needs to be addressed for nerve agent detection is selectivity, not just between different nerve agent classes⁵⁶, but also from potential sources of false-positive responses. For example, nitrogen-containing nucleophiles are bases and so, in principle, simple acids could also cause a change in the fluorescence signal and hence act as interferents.

The role of acids as interferents is important, particularly for the G-series nerve agents that contain a fluorine-phosphorus bond (e.g., Sarin, Soman, and cyclosarin). The fluorine-phosphorus bond is susceptible to hydrolysis to form an organophosphoric acid and hydrofluoric acid⁵⁷ and in fact, hydrofluoric acid is a known contaminant in as-prepared nerve agents⁵⁸. Furthermore, given the toxicity of nerve agents and their restricted availability, the efficacy of new sensing materials is generally tested against simulants that have lower toxicity. The reported simulants used for Sarin, Soman, and cyclosarin detection are diethylchlorophosphate (DCP) and di-*iso*-propyl-fluorophosphate (DFP), with the former being the more widely used. Studies of the hydrolysis of DFP⁵⁹ and DCP⁶⁰ show that DFP reacts with water within a few hours, with the process accelerating when the measurements were done in glass containers^{61,62}, while DCP reacts more quickly due to the weaker phosphorus-chlorine bond⁶⁰.

When surveying the literature on the fluorescence-based detection of G-series nerve agents and simulants a number of observations can be made, particularly of the pyridyl-containing sensing materials that are the focus of this study. First, in many cases, the response of the sensing material to DCP and hydrochloric acid/hydrogen chloride (and indeed other acids) is the same. Second, the source and/or quality of the simulant is not described. Third, there is a significant number of publications that state that the product of the sensing process is the pyridinium

hydrochloride salt that is formed via a phosphorylated intermediate. In most cases, no evidence is provided for the intermediate and it is assumed that hydrolysis occurs to give the salt. In the small number of cases where there is some apparent evidence, the measurements are undertaken in solution but without any indication of the kinetics of the reaction. Finally, given that solid-state reactions can be slower than those in solution there is an interesting question as to whether what is observed in solution is relevant for film-based detection, which is required for real time in field testing. That is, the solid-state response may be dominated by the acid impurity rather than the more complex multistep process of simulant diffusion into the film, phosphorylation, and hydrolysis.

Our current work was inspired by the need to develop a fundamental understanding of the role of acid as a potential interferent, particularly for sensing materials that contain the pyridyl moiety (or its fused ring analogs), which constitute around 50% of the reports at this time^{19–30,42–46}. In the first part of the study, we explore a conceptually elegant substitution-cyclisation strategy for the detection of G-series CWAs. For example, it has been previously reported that 1-hydroxymethyl-8-(pyrid-2-yl)naphthalene **1** (Fig. 1) can be used to rapidly detect DCP and DFP⁴⁶. The proposed mechanism involved the reaction of the primary alcohol to form a phosphate ester, followed by cyclisation to give pyridinium salt **1'** (Fig. 1). There have been a number of subsequent reports using this strategy^{40–51} although it has been noted that the pyridyl unit is susceptible to acid impurities. In investigating this strategy we replace the pyridyl moiety with a thiazolyl unit (**2** in Fig. 1) to compare the sensing efficacy and in so doing demonstrate the effect of acid impurities in the simulants on the detection process. The thiazolyl unit was chosen as the Ka of its conjugate acid is almost three orders of magnitude lower than pyridine (pKa = 2.5 versus 5.2) and, hence, should be less susceptible to acid interferents. We then expand the investigation to sensing materials that incorporate pyridyl groups more broadly (**3** and **4**, Fig. 1).

We show that if the Sarin or simulant is acid free there is no prompt response (change in the fluorescence) although there is a slow delayed response commensurate with the degradation of the simulant via hydrolysis under the measurement conditions. Our results are consistent with the view that the prompt fluorescence response of the sensing films upon Sarin or simulant vapor exposure is the result of protonation of the sensing material by acid impurities in the analyte, rather than the previously-proposed phosphorylation reaction pathways. Thus, it is important to carefully reconsider many of the reported sensors for the phosphonofluoridate G-series nerve agents and the effect of acid false positives.

Results and discussion

Purity and stability of the simulants. In the first part of this study, we investigated the purity and stability of DFP under different storage conditions. The DFP was synthesized following a reported procedure using di-*iso*-propylphosphite, cupric chloride, and cesium fluoride⁶³, with the material purified by Kügelrohr (bulb-to-bulb) distillation (fresh DFP – experimental note: a tube filled with potassium carbonate and two cold traps were placed between the vacuum pump and Kügelrohr distillation apparatus to protect the pump). The synthesized DFP was sealed in a plastic bottle and stored at $-20\text{ }^{\circ}\text{C}$ for 14 days or 143 days (non-treated and aged, respectively), or stored over the acid scavenger, hexamethylenetetramine (HMTA – 20 mg HMTA was added to 200 μL DFP), for 240 days at $-20\text{ }^{\circ}\text{C}$. The ^{31}P NMR spectra (Fig. 2a) of the freshly prepared DFP had a doublet at $\delta = -10.71$ ppm corresponding to the signal of the phosphorus atom with

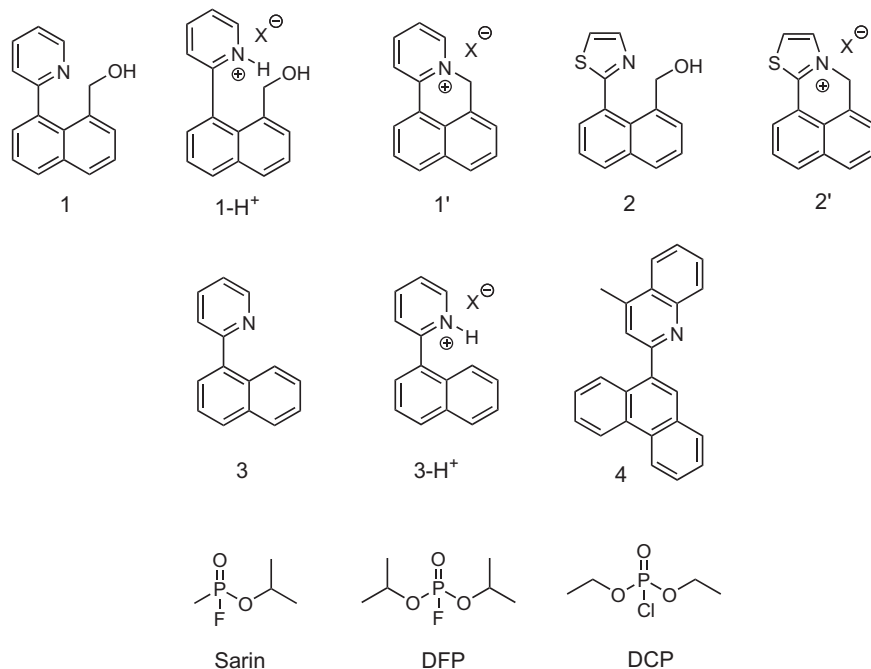


Fig. 1 Structures of the sensing compounds, proposed products and analytes. Structures of compounds **1**, **2**, **3** and **4**, the protonated forms **1-H⁺** and **3-H⁺**, the proposed cyclised products **1'** and **2'**, the analyte Sarin and its two simulants DFP and DCP. X is the counterion formed from the analyte vapor used.

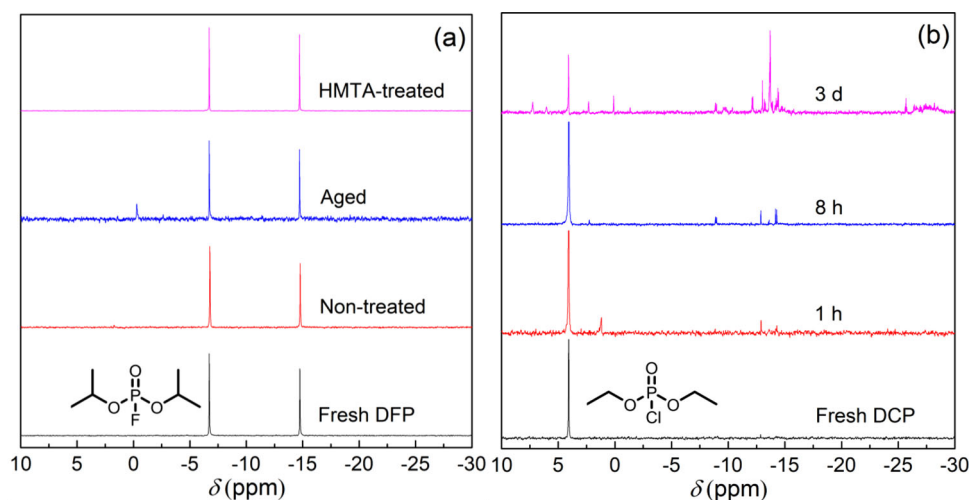


Fig. 2 ³¹P NMR spectra of DFP and DCP. **a** Fresh DFP, non-treated DFP (stored for 14 days), aged DFP (stored for 143 days) and HMTA-treated DFP (stored for 240 days); **b** Fresh DCP, and DCP stored in a capped glass vial for 1 h, 8 h, and 3 d without inert gas protection. The spectra were measured in dichloromethane-d₂.

fluorine coupling ($J_{P-F} = 972.8$ Hz). No change in the spectrum was observed for the DFP stored over HTMA, even after 8 months. In contrast, the aged DFP stored at the same temperature was found to have a clear extra peak in the ³¹P NMR spectrum that corresponded to di-*iso*-propylphosphoric acid ($\delta = -0.31$ ppm). It should be noted that given the sensitivity of ³¹P NMR it is possible that freshly prepared DFP also contained trace amounts of acid impurities. We found that acid impurities could be removed by treatment of the DFP with anhydrous potassium carbonate (10 wt%) for 30 min prior to an NMR measurement. However, DFP could not be stored over anhydrous potassium carbonate, with gel-like impurities forming on the surface of the particles during storage at -20 °C.

Based on the P-Cl and P-F bond strengths it would be expected that DCP would be more susceptible to hydrolysis than DFP. A previous ³¹P NMR study on the hydrolysis of DCP showed that when water was in excess diethyl phosphoric acid was formed, but when the DCP was used in large excess then multiple products corresponding to the phosphate monomer (³¹P NMR $-5.00 \sim 5.00$ ppm), pyrophosphate dimer (³¹P NMR $-20.00 \sim -5.00$ ppm) and poly(phosphate) trimer (³¹P NMR $-30.00 \sim -25.00$ ppm) were observed⁶⁰. DCP is often used under ambient conditions. We, therefore, investigated the stability of DCP to ambient moisture by placing 200 μ L of freshly distilled DCP stored in a glass vial (2 mL) that had been capped under normal laboratory environmental conditions, that is room

temperature with the relative humidity being around 50–60%. The ^{31}P NMR of the DCP was measured over intervals of time with the results shown in Fig. 2b. Freshly distilled DCP had a peak at 4.06 ppm, but after an hour, extra signals in the ^{31}P NMR were observed. These signals continued to grow over time and were consistent with the previously reported hydrolyzed products⁶⁰. In this experiment, DCP absorbs water from the

atmosphere and so DCP is always present in large excess relative to water. The fact that phosphorous impurities form means that hydrochloric acid will also be present in the DCP.

These results demonstrate the importance of knowing the storage history of DFP and DCP when testing new fluorescence-based sensing materials that are capable of acting as a Brønsted or Lewis base. Failure to do so could lead to acid impurities giving a

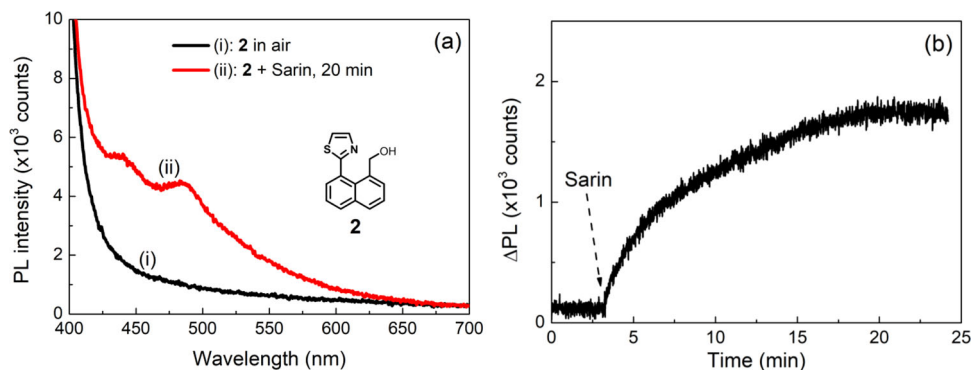


Fig. 3 PL response of sensing compound 2 to Sarin. PL spectra (a) and time-dependence (b) of solid-state films with **2** in cellulose acetate before and after the introduction and continuous exposure to the vapor of a stored Sarin sample. A 365 nm LED was used to excite the film. The PL spectra were recorded on an OceanOptics Flame spectrometer and were not corrected. The PL signal in the absence of Sarin in **a** is due to the tail of the excitation. For the PL time-dependence, the intensity of the emission peak at 484 nm was recorded and the data has been corrected for the scattered excitation.

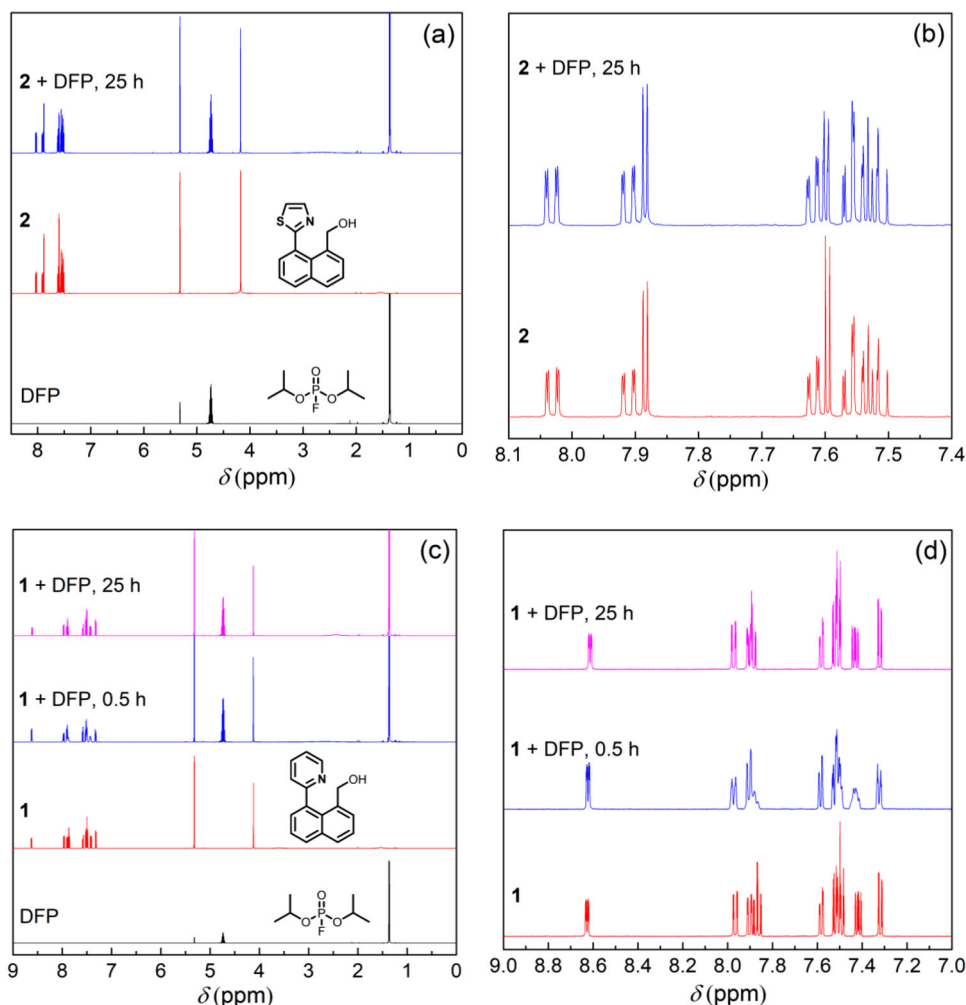


Fig. 4 ^1H NMR spectra of the sensing compounds upon addition of DFP. Spectra of **2** (a full spectrum; b aromatic region) and **1** (c full spectrum; d aromatic region) with addition of DFP (1 eq) in dichloromethane- d_2 . All experiments were carried out at room temperature.

false positive response to a simulant, even when the acid is present at very low levels. It should be noted that the impurity and storage of DFP can also be influenced by the synthetic method. For example, DFP synthesized with di-*iso*-propyl phosphite, potassium fluoride and 1,3-dichloro-5,5-dimethylhydantoin has been reported to show better storage stability than commercial DFP⁶¹.

Thin-film sensing of Sarin, DFP, and DCP vapors. Following the method reported for vapor detection using **1** we prepared thin films containing 10 wt% of **2** (see Supplementary Methods for the synthetic route) in cellulose acetate for the detection of Sarin vapor. The as-prepared film was found to be non-emissive when excited at 365 nm (note that **2** does not absorb at this wavelength) (Fig. 3a, curve i) but when exposed to the vapor of Sarin that had been stored, a new emission peak at 484 nm was observed (Fig. 3a, curve ii), with the photoluminescence (PL) intensity showing a gradual increase over time (Fig. 3b).

Based on the solution-based measurements reported for **1** in the presence of DCP and DFP, the fluorescence turn-on observed for the film containing **2** would be consistent with it undergoing a rapid nucleophilic substitution-cyclisation process akin to **1** being converted to **1'**. To confirm this was indeed the case, we followed the reaction of **2** with one equivalent of freshly prepared DFP (acid-free) using solution ¹H NMR (Fig. 4a: full spectrum; Fig. 4b: aromatic region). Given the rapidity of the film response to Sarin we were surprised to find that even after 25 h no new ¹H NMR peaks corresponding to the cyclised product were observed. Thus, while there appeared to be a rapid response to Sarin vapor in the film, in solution the reaction with the simulant was essentially non-existent. The results are counter to what would normally be expected, that is, solution-based chemical transformations are often faster than those in the solid-state, particularly when there is a significant requirement for structural rearrangement.

It was therefore deemed critical to determine why we observed an increase in the PL with Sarin and no chemical transformation for DFP in solution. The relative electrophilicities of DFP and Sarin could be one source of the response difference and to confirm whether this was the case we compared the response of a solution of **2** with that of **1**, which has been reported to react with DFP both in solution and film⁴⁶. As stated earlier the *K_a* of the conjugate acid of thiazole is three orders of magnitude lower than that of pyridine and hence the nitrogen of **2** is less nucleophilic than that of **1**. Furthermore, the cyclisation product from **2** would be expected to have a higher ring strain, which could also explain its lack of formation as compared to **1**. However, it should be noted that the ¹H NMR experiment appeared to show that the first step, the reaction with the benzylalcohol of **2**, had also not occurred. We, therefore, carried out the same ¹H NMR experiment with **1** as the sensing compound, with the results shown in Fig. 4c (Fig. 4d: aromatic region). Again, no new peaks corresponding to the cyclised product (in this case **1'** with X = F) were observed after 25 h, which is inconsistent with the reported rapid change in fluorescence both in solution and film⁴⁶.

These ¹H NMR experiments clearly showed that neither **1** or **2** undergo an appreciable chemical transformation with DFP and hence the change in fluorescence shown in Fig. 3 must arise from a different process. As described earlier, both DFP and DCP are known to hydrolyze to give hydrofluoric and hydrochloric acid, respectively, and the presence of acid could potentially be the source of the observed change in fluorescence of the films when exposed to Sarin. We, therefore, exposed **1**:cellulose acetate blend films to vapors of DFP that had been stored and/or treated under different conditions. Compound **1** was chosen to enable direct comparison with the previously reported results⁴⁶. When the

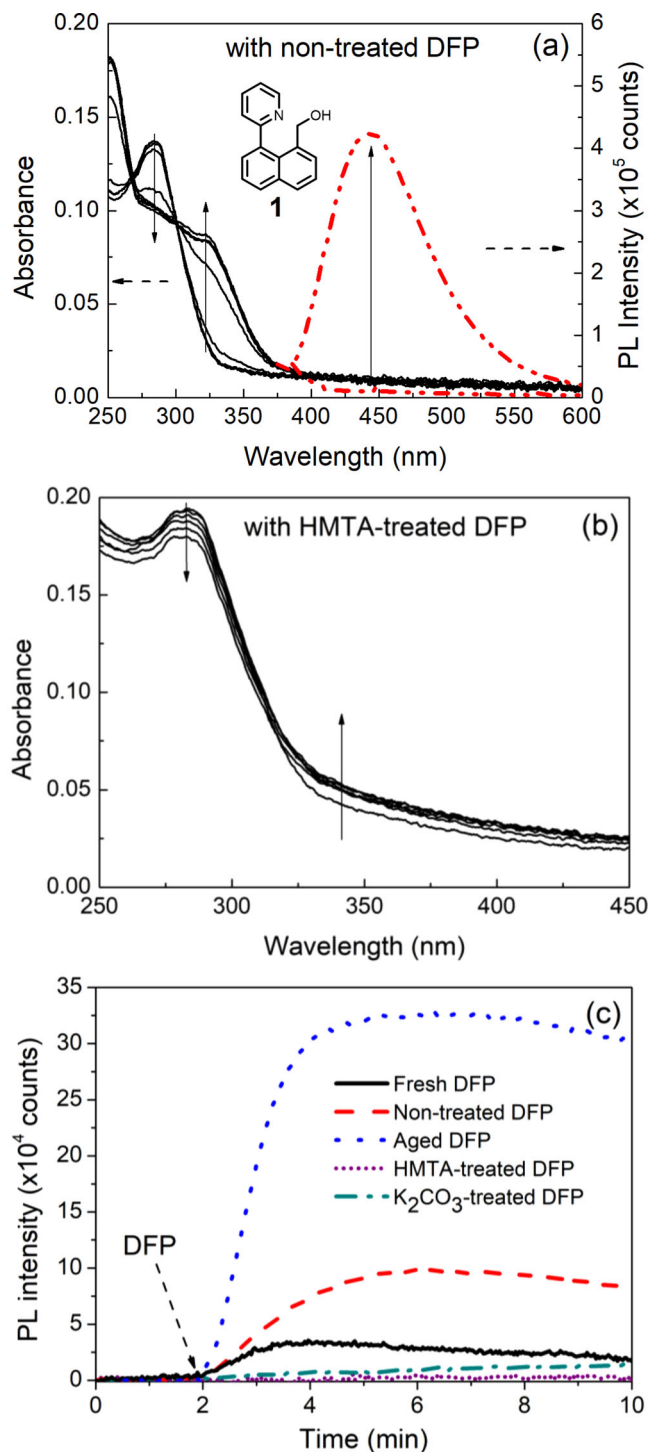


Fig. 5 Sensing results of compound **1** upon exposure to differently treated DFP. **a** UV-vis absorption and PL spectra (excitation wavelength = 365 nm) of 10 wt% **1**:cellulose acetate films upon exposure to non-treated DFP (0–4 min); **b** UV-vis absorption spectra of the films upon exposure to HMTA-treated DFP (0–10 min); **c** Representative PL kinetics curves for the sensing films against various DFP sources. The PL spectra in **a** were recorded using an FS5 spectrometer and the PL kinetics in **c** were recorded using an OceanOptics Flame spectrometer using the setup described in Supplementary Fig. S2a.

10 wt% **1**:cellulose blend film was exposed to non-treated DFP (stored at -20°C for 14 days) the absorption spectrum was red shifted with a new peak at 322 nm and the onset shifted from ~ 350 nm to ~ 400 nm (Fig. 5a). In addition, fluorescence turn-on

at 444 nm was observed (excitation wavelength = 365 nm) (Fig. 5a). It should be noted that a similar response was achieved when **1** was blended with cellulose acetate at a 1 wt% concentration (Supplementary Fig. S1). When the vapor from freshly prepared DFP was used there was a much smaller increase in the fluorescence than that of the aged-DFP (143 days of storage) (Fig. 5c). The acid-free HMTA-treated DFP showed no observable changes in either the absorption (Fig. 5b) or PL spectra (Fig. 5c). The difference in magnitude of these responses was consistent with acid being present in the DFP based on the hydrolysis products observed in the ^{31}P NMR spectra (Fig. 2). Thus, combining the results from the ^1H NMR and film PL measurements strongly suggests that neither **1** and **2** are responding to Sarin or the simulant but rather the acids formed from their hydrolysis.

We also carried out a similar series of experiments with DCP, which as described earlier is known to hydrolyze faster than DFP. The DCP was purified by distillation and stored in a nitrogen-filled glovebox. We first performed the sensing measurement under an inert atmosphere. The DCP vapor was generated by bubbling nitrogen through DCP liquid (Supplementary Fig. S2b). When films of **1**:cellulose blends were exposed to the glovebox-stored DCP vapor a rapid fluorescence turn-on (within 30 s) was observed, as shown in Fig. 6a. Even though we took care to store the DCP under anhydrous conditions, we were concerned that the rapid increase in fluorescence could be due to acid impurities formed during storage or transfer. To test this, we added anhydrous potassium carbonate to the DCP, which was then stirred for 30 min before use. Repeating the experiment with the potassium carbonate-treated DCP under the same conditions as before led to no observable change in fluorescence (Fig. 6a),

confirming that removing the acid impurities from DCP is critical. An important side observation from this experiment is that it shows that the reaction between DCP and the hydroxyl groups of the cellulose acetate is slow relative to the sensing process in the solid-state. In a final experiment, we investigated the ability of the **1**:cellulose films to sense DCP in air. Using a similar method to that of the DFP experiments, the DCP was placed at the bottom of the optical sensing chamber in air (Supplementary Figure S2a), and the change in fluorescence measured over time. As shown in Fig. 6b, when carrying out the measurements immediately using freshly distilled DCP (curve i) or DCP stored over potassium carbonate (curve ii) a fluorescence turn-on response was observed, although the change was relatively slow (curve i). If the DCP was left in the chamber in air for 30 min to an hour before the measurement, then the change in fluorescence was rapid (curves iii and iv, respectively). These results indicate that DCP rapidly reacts with moisture in the air and that the results from measurements undertaken under such conditions should be treated with caution and potentially re-evaluated.

In a further set of experiments to confirm that the change in fluorescence observed for **1**, and by analogy **2**, was due to acid and not the simulant, we prepared the protonated product **1-H⁺** (X = Cl) and the fully cyclised compound **1'** (X = Br) (see Supplementary Methods for the synthetic procedures and Supplementary Figs. S3 and S4 for ^1H NMR analysis of the structures). We also prepared **3-H⁺** that lacked the alcohol group required for the initial nucleophilic substitution step with the simulant and its protonated form **3-H⁺** (X = Cl). Figure 7 shows the absorption (Fig. 7a) and PL (Fig. 7b) spectra of the compounds in acetonitrile. In Fig. 7a it can be clearly seen that

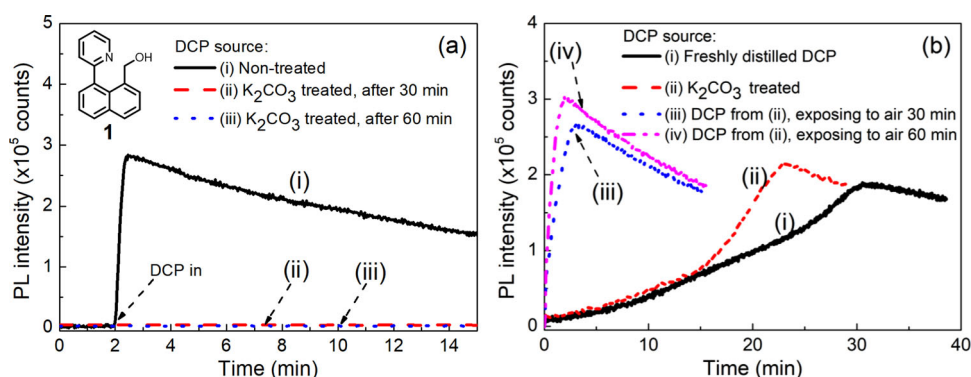


Fig. 6 Sensing results of compound **1 upon exposure to differently treated DCP.** Representative PL kinetics curves for 10 wt% **1**:cellulose acetate sensing films under (a) a nitrogen flow containing non-treated DCP or potassium carbonate-treated DCP (30 or 60 minutes), and (b) an air atmosphere with freshly distilled DCP (curve i), potassium carbonate-treated DCP (curve ii), and potassium carbonate-treated DCP left in air for 30 (curve iii) and 60 min (curve iv). The PL kinetics were recorded using an OceanOptics Flame spectrometer.

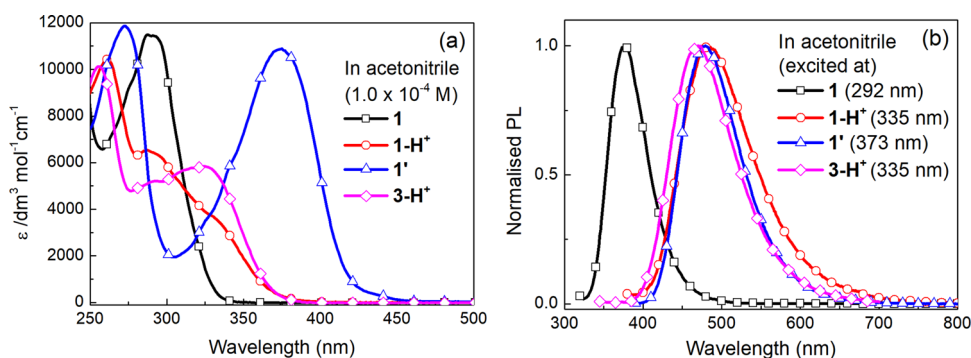


Fig. 7 The optical properties of **1, **1-H⁺**, **1'**, and **3-H⁺** in acetonitrile.** a UV-vis and b PL spectra.

the onset of the absorption spectrum of 1-H^+ ($X = \text{Cl}$) is red-shifted compared to 1 and similar to that of 3-H^+ ($X = \text{Cl}$). However, the long-wavelength components of the absorption spectra of the protonated compounds are significantly blue-shifted when compared with the cyclised compound $1'$ ($X = \text{Br}$) whose absorption peak was at 374 nm. It is interesting to note that the PL spectra of 1-H^+ ($X = \text{Cl}$), 3-H^+ ($X = \text{Cl}$), and $1'$ ($X = \text{Br}$) are at similar wavelengths but red-shifted compared to 1 . It should also be noted that the protonated and cyclised compounds showed a solvchromatic effect (see Supplementary Fig. S5), which needs to be considered when comparing results with published reports and solid-state measurements.

The optical properties of the compounds in cellulose acetate films were then investigated and compared with the films of 1 exposed to aged DFP or non-treated DCP (Fig. 8). The concentration of 1 or 3-H^+ ($X = \text{Cl}$) was 10 wt% (in a similar manner to the sensing measurements shown in Fig. 6). However, due to solubility limitations and the need to have optically clear films for the UV-vis absorption measurements, the concentrations of 1-H^+ ($X = \text{Cl}$) and $1'$ ($X = \text{Br}$) were 2 and 5 wt%, respectively. Figure 8a shows that the absorption maximum of $1'$ ($X = \text{Br}$) was at the longest wavelength in a similar manner to the solution measurements. Importantly, the absorption spectra of the films of 1 exposed to aged DFP and non-treated DCP were similar to that of the 1-H^+ ($X = \text{Cl}$):cellulose acetate and 3-H^+ ($X = \text{Cl}$):cellulose acetate films but significantly different to the $1'$:cellulose acetate film. Likewise, the PL spectra (Fig. 8b) of the 1 :cellulose acetate films exposed to aged DFP or non-treated DCP were similar to that of the 1-H^+ ($X = \text{Cl}$):cellulose acetate film, with the peak blue-shifted compared to the cyclized $1'$:cellulose acetate film. The excitation spectra (Fig. 8c) provide further spectroscopic evidence that the fluorescence turn on is due to protonation and not cyclisation. The excitation spectra were measured at an emission wavelength of 450 nm and it can be clearly seen that the spectra of the 1 :cellulose acetate films exposed to aged DFP or non-treated DCP are the same as those of the 1-H^+ :cellulose acetate films and different to the spectrum of the $1'$:cellulose acetate film.

When these photophysical results are taken in conjunction with the NMR data shown in Fig. 4 and the sensing measurements shown in Figs. 5c and 6a where there was no PL response for 1 :cellulose acetate films exposed to potassium carbonate or hexamethylenetetramine treated DFP or potassium carbonate-treated DCP the logical conclusion is that protonation due to acid impurities in the DFP and DCP is the cause of the rapid change in the fluorescence.

We also prepared the cyclised compound $2'$ ($X = \text{Br}$) from 2 to confirm the difference in the photophysical properties we observed between 1 and $1'$. It should be noted that the low pKa (2.5) of the conjugate acid of thiazole meant we could not isolate protonated 2 . The emission and excitation spectra of films of 2 (before and after treatment with aged DFP or hydrogen chloride) and $2'$ blended with cellulose acetate are shown in Fig. 9. The PL spectrum of the film containing $2'$ was red shifted compared to those of the 2 :cellulose acetate films when exposed to aged DFP and hydrogen chloride (Fig. 9a). However, the excitation spectrum provides additional clear evidence that the increase in the fluorescence is due to protonation of 2 and not cyclisation to form $2'$ (Fig. 9b). It can be clearly seen that the excitation spectrum at an emission wavelength of 450 nm of $2'$ ($X = \text{Br}$) is significantly red-shifted compared to the films that had been treated with the aged DFP and hydrogen chloride, which were essentially the same. That is, the PL shown in Fig. 9a arises from the protonation of 2 .

There are a significant number of sensing materials that contain the pyridyl moiety (and fused heteroaromatic rings such as

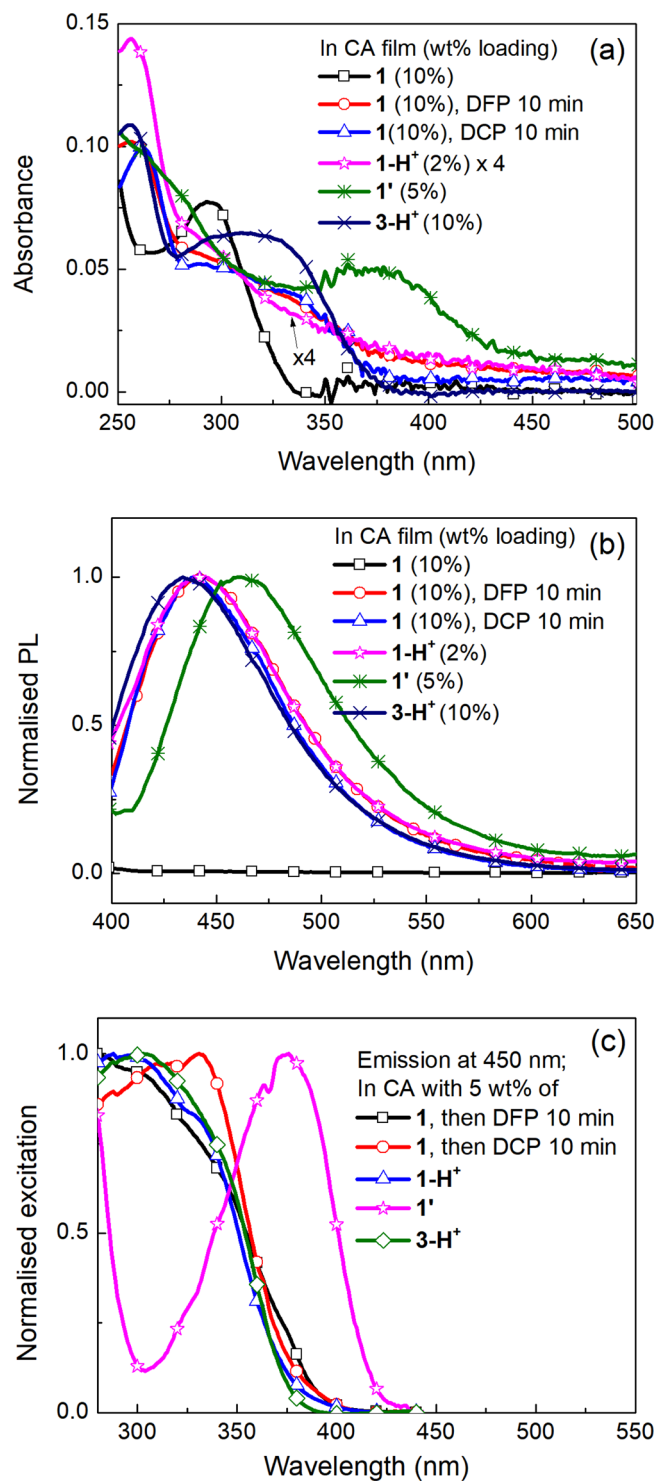


Fig. 8 The optical properties of 1 , 1-H^+ , $1'$, and 3-H^+ :cellulose acetate films compared to 1 :cellulose acetate films upon exposure to aged DFP or non-treated DCP vapor. **a** UV-vis, **b** emission (excitation wavelength = 365 nm), and **c** excitation spectra measured for an emission wavelength of 450 nm.

quinoline and quinoxaline) that do not require the cyclisation step. We, therefore, explored 3 and 4 ⁶⁵ for the solid-state detection of Sarin and/or DFP and DCP vapor that either contained acid or were acid-free with the results shown in Fig. 10. It can be seen that both 3 and 4 :cellulose acetate blend sensing films showed a sharp fluorescence turn-on response when they were exposed to either

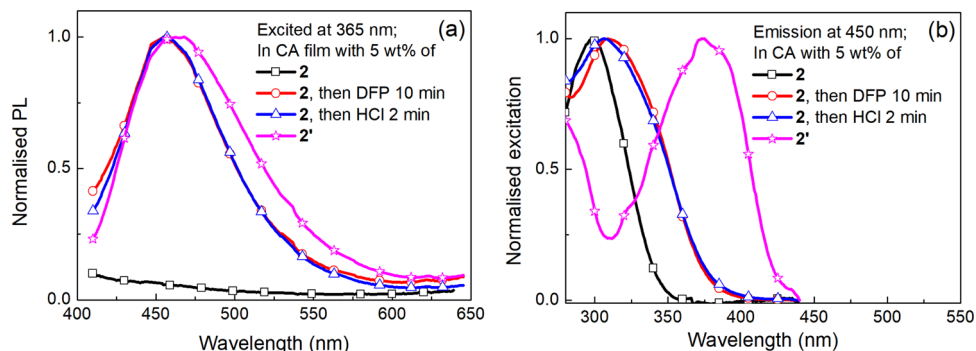


Fig. 9 The optical properties of **2** and **2'**:cellulose acetate films compared to **2**:cellulose acetate films upon exposure to aged DFP or hydrogen chloride vapor. **a** PL emission and **b** excitation spectra. PL spectra were recorded using an FS5 spectrometer. DFP and HCl vapor were generated using the setup described in Supplementary Fig. S2a.

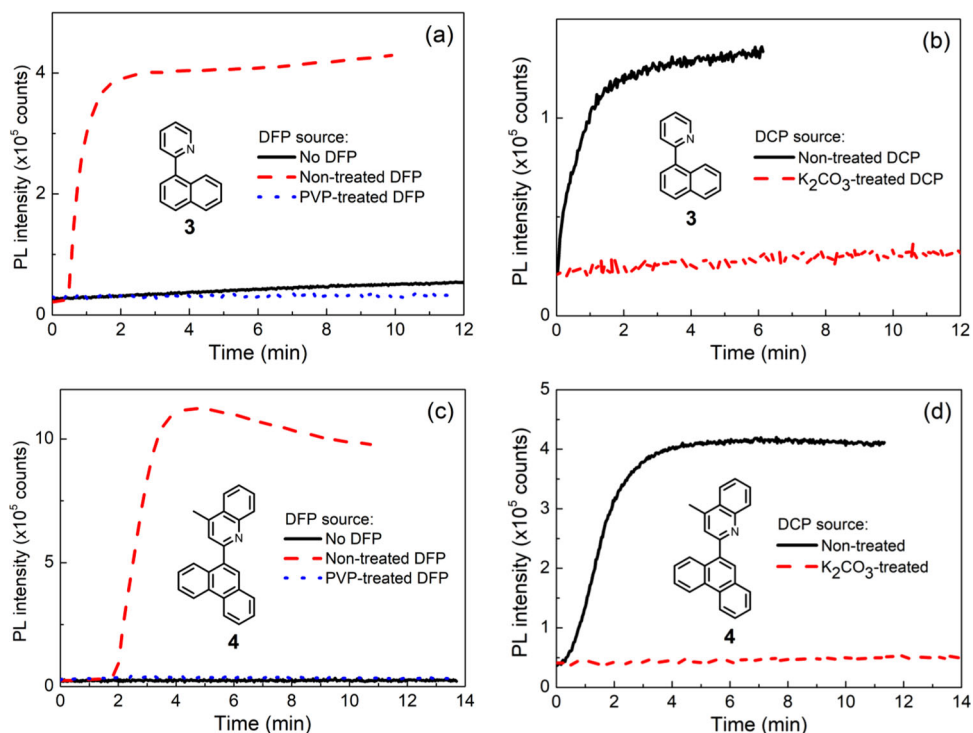


Fig. 10 Sensing results of compounds **3** and **4** upon exposure to differently treated DFP and DCP. Representative PL kinetics curves for **(a, b)** 10 wt% **3**: cellulose acetate sensing films and **(c, d)** 10 wt% **4**:cellulose acetate sensing films exposed to acid free and impure DFP and DCP sources. The set-up shown in Supplementary Fig. S2a was used for measurements with DFP with that of Supplementary Fig. S2b used for DCP. Non-treated DFP was stored at -20°C for 3 months; PVP-treated DFP was prepared by adding 20 mg of poly(4-vinylpyridine) (PVP) to 200 μL of DFP; Non-treated DCP was stored in a glovebox; potassium carbonate-treated DCP was prepared by adding 200 mg of potassium carbonate to 1 mL of DCP. The PL kinetics were recorded using an OceanOptics Flame spectrometer.

non-treated DFP or DCP (Fig. 10a: **3** with DFP; Fig. 10b: **3** with DCP; Fig. 10c: **4** with DFP; Fig. 10d: **4** with DCP). Comparison of the response of the **4** containing films to DCP or hydrogen chloride shows that the PL spectra of both films were identical (Supplementary Fig. S6). However, when DFP and DCP were treated with poly(4-vinylpyridine) (PVP) and anhydrous potassium carbonate, respectively, no response (Fig. 10a, c with DFP) or a very slow (Fig. 10b, d with DCP) change in the fluorescence was observed. These results are in agreement with the fluorescence response from compound **1** (Fig. 5c with DFP and Fig. 6a with DCP) and are evidence that the observed sharp fluorescence turn-on response with non-treated DFP and DCP is due to the acid impurities. Thus it is reasonable to conclude that published sensing materials containing pyridyl-like moieties detect the acid

impurities rather than DFP or DCP themselves. Interestingly, nearly 20 years ago a ^{31}P NMR study showed that the rate of reaction between pyridine and diethyl chlorophosphate was slow with the equilibrium strongly to the left⁶⁶. Furthermore, they found changes in the ^{31}P NMR spectra occurred more rapidly in the presence of water. Thus, while it may be possible for a phosphoropyridinium intermediate to form in solution it is unlikely to be responsible for the rapid observable fluorescence changes in the detection of the vapors by sensing films. That is, the lack of response when **3** or **4** were blended with hydroxyl-containing cellulose acetate and exposed to base-treated (acid free) DFP or DCP was because the phosphoropyridinium intermediate and its subsequent hydrolysis by adventitious water simply does not occur on the time scale of the measurement.

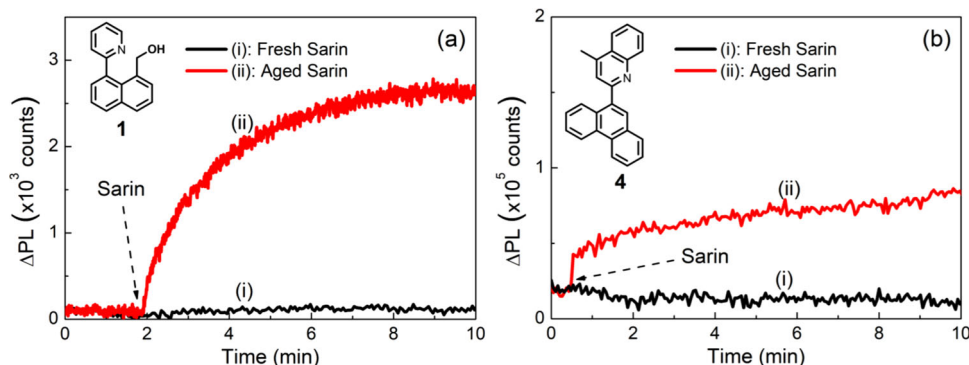


Fig. 11 Sensing results of films of **1** and **4** upon exposure to freshly prepared and aged Sarin. Representative PL kinetics curves for (a) 10 wt% **1**:cellulose acetate and (b) 10 wt% **4**:cellulose acetate sensing films exposed to vapors of aged (being stored for more than 6 months) and fresh (prepared and distilled twice less than one week before use) Sarin using the Supplementary Fig. S2a setup. The PL kinetics were recorded using an OceanOptics Flame spectrometer.

Finally, to confirm that what we observed for the pyridyl-containing compounds with or without hydroxyl group, was not an artifact of the CWA simulants (DFP and DCP) we also tested films containing **1** and **4** against Sarin with different storage histories. The Sarin used was either aged (being stored for more than 6 months) or freshly synthesized (less than one week before use). As shown in Fig. 11, a fluorescence turn-on response was observed with the aged Sarin while there was no response for both compounds **1** and **4** when freshly prepared Sarin was used. Thus, these results further confirm that phosphorylation of the pyridyl-containing compounds is not the major mechanism for fluorescence detection of the G-series CWAs and their simulants.

Conclusion

Drawing these results together, we have investigated sensing compounds that were designed with functionality to undergo a substitution or substitution-cyclisation pathway for the detection of phosphonofluoridate G-series nerve agents and simulants. The results show that the fast fluorescence response of the sensing thin films upon Sarin, DFP or DCP vapor exposure are the result of simple protonation of the sensing material by acid in the analyte, rather than the previously-proposed phosphorylation and/or subsequent cyclisation. Indeed, in solution the sensing materials can detect acid at a concentration as low as 0.4 μM (Supplementary Fig. S7). Thus, these findings have significant implications for many of the developed sensing materials which have nucleophilic groups that are also basic and hence it is important to carefully reconsider the effect of acid false positives. Indeed it is of concern that the fluorescence responses of many of the reported sensors for the phosphonofluoridate G-series nerve agents may simply be caused by the presence of acid impurities in the simulant, particularly for solid-state detection of CWA vapors. We believe that the findings described here will stimulate the ongoing search for truly selective chemosensors for nerve agents.

Methods

Film preparation. The sensing compound was dissolved in ethanol (1–10 mg/mL). Cellulose acetate (Sigma-Aldrich, average $M_n \sim 30,000$ by GPC, 39.8 wt% acetyl) was dissolved in acetone (20 mg/mL). Then 200 μL of sensing compound in ethanol was mixed with 900 μL of cellulose acetate in acetone and the resulting mixture was stirred at room temperature for 10 min. Thin films were prepared on fused silica substrates by spin-coating at 2000 rpm for 60 s to give a thickness of ≈ 220 nm.

Sensing measurements. *Caution:* Dialkylfluorophosphates are highly toxic compounds. They should only be synthesized, purified, used and disposed of after rigorous risk assessment. All processes should only be undertaken by trained

persons using appropriate personal protection equipment. *Disclaimer:* Work with Schedule 1 CWAs should only be performed at OPCW declared facilities. The sensing film samples on fused silica substrates were mounted in a closed sample chamber which was connected via optical fibers to an LED light source (365 nm, OceanOptics) and a spectrometer (Flame, OceanOptics). The sample chamber featured three optical windows to allow for excitation of the films and subsequent detection of the film PL at right angles to the excitation. For experiments conducted in air (see Supplementary Fig. S2a for the experimental setup), 2 μL of DFP, DCP or hydrochloric acid (16%) was placed on the surface of a Teflon lid, which was placed at the bottom of the chamber or a pipette droplet of Sarin was added directly into the bottom of the chamber. Evaporation at 20–22 $^{\circ}\text{C}$ gave the analyte vapor. Film PL spectra before and after exposure to the analyte were recorded using an OceanOptics Flame spectrometer whose spectral response was not corrected or an FS5 spectrometer whose spectral response was corrected. PL kinetics at the emissive peak were recorded on the Flame spectrometer through OceanView software (OceanOptics). Due to the fast hydrolysis of DCP with moisture, sensing experiments with DCP were also carried out under a nitrogen flow (see Supplementary Fig. S2b for the experimental setup). Specifically, a mixture of DCP (1 mL) and anhydrous potassium carbonate (200 mg) was stirred in a 10-mL Schlenk tube at room temperature under nitrogen for 30 min. Then nitrogen (100 mL/min) was bubbled through the liquid DCP to generate the vapor, which was then diluted using a second nitrogen flow (200 mL/min), before being introduced into the optical chamber for the sensing measurement. The nitrogen stream was then passed through a scrubbing solution (20 wt% sodium hydroxide in water) to break down the excess simulant.

Data availability

The authors declare that data and experimental methods supporting the findings of this study are available in the Supplementary file. Unrestricted data is available from the authors upon reasonable request.

Received: 4 November 2020; Accepted: 26 February 2021;

Published online: 26 March 2021

References

- Costanzi, S., Machado, J.-H. & Mitchell, M. Nerve agents: what they are, how they work, how to counter them. *ACS Chem. Neurosci.* **9**, 873–885 (2018).
- Delfino, R. T., Ribeiro, T. S. & Figueroa-Villar, J. D. Organophosphorus compounds as chemical warfare agents: a review. *J. Braz. Chem. Soc.* **20**, 407–428 (2009).
- Valdez, C. A., Leif, R. N., Hok, S. & Hart, B. R. Analysis of chemical warfare agents by gas chromatography-mass spectrometry: methods for their direct detection and derivatization approaches for the analysis of their degradation products. *Rev. Anal. Chem.* **37**, <https://doi.org/10.1515/revac-2017-0007> (2018).
- Matějovský, L. & IPitschmann, V. New carrier made from glass nanofibres for the colorimetric biosensor of cholinesterase inhibitors. *Biosensors* **8**, 51 (2018).
- Walker, J. P. & Asher, S. A. Acetylcholinesterase-based organophosphate nerve agent sensing photonic crystal. *Anal. Chem.* **77**, 1596–1600 (2005).
- Liu, G. & Lin, Y. Biosensor based on self-assembling acetylcholinesterase on carbon nanotubes for flow injection/amperometric detection of organophosphate pesticides and nerve agents. *Anal. Chem.* **78**, 835–843 (2006).

7. Fennell, J. F., Hamaguchi, H., Yoon, B. & Swager, T. M. Chemiresistor devices for chemical warfare agent detection based on polymer wrapped single-walled carbon nanotubes. *Sensors* **17**, 982 (2017).
8. Zhu, R., Azzarelli, J. M. & Swager, T. M. Wireless hazard badges to detect nerve-agent simulants. *Angew. Chem. Int. Ed.* **55**, 9662–9666 (2016).
9. Saetia, K. et al. Spray-layer-by-layer carbon nanotube/electrospun fiber electrodes for flexible chemiresistive sensor applications. *Adv. Func. Mater.* **24**, 492–502 (2014).
10. Yang, Y., Ji, H.-F. & Thundat, T. Nerve agents detection using a Cu²⁺/l-cysteine bilayer-coated microcantilever. *J. Am. Chem. Soc.* **125**, 1124–1125 (2003).
11. Hartmann-Thompson, C. et al. Hydrogen-bond acidic hyperbranched polymers for surface acoustic wave (SAW) sensors. *Chem. Mater.* **16**, 5357–5364 (2004).
12. Shaw, P. E. & Burn, P. L. Real-time fluorescence quenching-based detection of nitro-containing explosive vapors: what are the key processes? *Phys. Chem. Chem. Phys.* **19**, 29714–29730 (2017).
13. Sun, X., Wang, Y. & Lei, Y. Fluorescence based explosive detection: from mechanisms to sensory materials. *Chem. Soc. Rev.* **44**, 8019–8061 (2015).
14. Salinas, Y. et al. Optical chemosensors and reagents to detect explosives. *Chem. Soc. Rev.* **41**, 1261–1296 (2012).
15. Thomas, S. W., Joly, G. D. & Swager, T. M. Chemical sensors based on amplifying fluorescent conjugated polymers. *Chem. Rev.* **107**, 1339–1386 (2007).
16. Fan, S. et al. Challenges in fluorescence detection of chemical warfare agent vapors using solid-state films. *Adv. Mater.* **32**, 1905785 (2020).
17. Chen, L., Wu, D. & Yoon, J. Recent advances in the development of chromophore-based chemosensors for nerve agents and phosgene. *ACS Sens* **3**, 27–43 (2018).
18. Jang, Y. J., Kim, K., Tsay, O. G., Atwood, D. A. & Churchill, D. G. Update 1 of: destruction and detection of chemical warfare agents. *Chem. Rev.* **115**, PR1–PR76 (2015).
19. Jo, S. et al. Conjugated polymer dots-on-electrospun fibers as a fluorescent nanofibrous sensor for nerve gas stimulant. *ACS Appl. Mater. Interfaces* **6**, 22884–22893 (2014).
20. Cai, Y.-C., Li, C. & Song, Q.-H. Fluorescent chemosensors with varying degrees of intramolecular charge transfer for detection of a nerve agent mimic in solutions and in vapor. *ACS Sens* **2**, 834–841 (2017).
21. Yao, J. et al. Concise and efficient fluorescent probe via an intramolecular charge transfer for the chemical warfare agent mimic diethylchlorophosphate vapor detection. *Anal. Chem.* **88**, 2497–2501 (2016).
22. Sun, C. et al. Fast and ultrasensitive detection of a nerve agent simulant using carbazole-based nanofibers with amplified ratiometric fluorescence responses. *Anal. Chem.* **90**, 7131–7134 (2018).
23. Xiong, W., Gong, Y., Che, Y. & Zhao, J. Sensitive discrimination of nerve agent and sulfur mustard simulants using fluorescent coassembled nanofibers with Förster resonance energy transfer-enhanced photostability and emission. *Anal. Chem.* **91**, 1711–1714 (2019).
24. Li, X. et al. Visualization of ultrasensitive and recyclable dual-channel fluorescence sensors for chemical warfare-agents based on the state dehybridization of hybrid locally excited and charge transfer materials. *Anal. Chem.* **91**, 10927–10931 (2019).
25. Jiang, H. et al. Hyperbranched polymer based fluorescent probes for ppt level nerve agent simulant vapor detection. *Anal. Methods* **9**, 1748–1754 (2017).
26. Diaz de Greñu, B. et al. Fluorescent discrimination between traces of chemical warfare agents and their mimics. *J. Am. Chem. Soc.* **136**, 4125–4128 (2014).
27. Huang, S., Wu, Y., Zeng, F., Sun, L. & Wu, S. Handy ratiometric detection of gaseous nerve agents with AIE-fluorophore-based solid test strips. *J. Mater. Chem. C* **4**, 10105–10110 (2016).
28. Cai, Y. C., Li, C. & Song, Q. H. Selective and visual detection of a nerve agent mimic by phosphorylation and protonation of quinolin oximes. *J. Mater. Chem. C* **5**, 7337–7343 (2017).
29. Dagnaw, F. W., Feng, W. & Song, Q.-H. Selective and rapid detection of nerve agent simulants by polymer fibers with a fluorescent chemosensor in gas phase. *Sens. Actuat B-Chem.* **318**, 127937 (2020).
30. Kim, Y., Jang, Y. J., Lee, D., Kim, B.-S. & Churchill, D. G. Real nerve agent study assessing pyridyl reactivity: selective fluorogenic and colorimetric detection of soman and simulant. *Sens. Actuat B Chem.* **238**, 145–149 (2017).
31. Fu, Y. et al. Highly sensitive determination of 2,4,6-trichlorophenol by using a novel SiO₂@MIPIL fluorescence sensor with a double recognition functional monomer. *ACS Sens* **3**, 1445–1454 (2018).
32. Zeng, L. et al. A single fluorescent chemosensor for simultaneous discriminative detection of gaseous phosgene and a nerve agent mimic. *Anal. Chem.* **91**, 12070–12076 (2019).
33. Zhou, X., Zeng, Y., Liyan, C., Wu, X. & Yoon, J. A fluorescent sensor for dual-channel discrimination between phosgene and a nerve-gas mimic. *Angew. Chem. Int. Ed.* **55**, 4729–4733 (2016).
34. Singh, V. V. et al. Micromotor-based on-off fluorescence detection of sarin and soman simulants. *Chem. Commun.* **51**, 11190–11193 (2015).
35. Bencic-Nagale, S., Sternfeld, T. & Walt, D. R. Microbead chemical switches: an approach to detection of reactive organophosphate chemical warfare agent vapors. *J. Am. Chem. Soc.* **128**, 5041–5048 (2006).
36. Khan, M. S. J., Wang, Y.-W., Senge, M. O. & Peng, Y. Sensitive fluorescence on-off probes for the fast detection of a chemical warfare agent mimic. *J. Hazard. Mater.* **342**, 10–19 (2018).
37. Patra, L. et al. A selective fluorogenic chemosensor for visual detection of chemical warfare reagent mimic diethylchlorophosphate. *J. Photochem. Photobiol. A* **388**, 112188 (2020).
38. Gupta, M. & Lee, H. A dual responsive molecular probe for the efficient and selective detection of nerve agent mimics and copper (II) ions with controllable detection time. *Sens. Actuat B-Chem.* **242**, 977–982 (2017).
39. Kim, T.-I., Maity, S. B., Bouffard, J. & Kim, Y. Molecular rotors for the detection of chemical warfare agent simulants. *Anal. Chem.* **88**, 9259–9263 (2016).
40. Heo, G., Manivannan, R., Kim, H. & Son, Y.-A. Liquid and gaseous state visual detection of chemical warfare agent mimic DCP by optical sensor. *Dyes Pigments* **171**, 107712 (2019).
41. Gotor, R., Costero, A. M., Gaviña, P. & Gil, S. Ratiometric double channel borondipyrromethene based chemodosimeter for the selective detection of nerve agent mimics. *Dyes Pigments* **108**, 76–83 (2014).
42. Lloyd, E. P., Pilato, R. S. & Houten, K. A. V. Polymer-bound 4-pyridyl-5-hydroxyethyl-thiazole fluorescent chemosensors for the detection of organophosphate nerve agent simulants. *ACS Omega* **3**, 16028–16034 (2018).
43. Sarkar, S. & Shunmugam, R. Polynorbornene derived 8-hydroxyquinoline paper strips for ultrasensitive chemical nerve agent surrogate sensing. *Chem. Commun.* **50**, 8511–8513 (2014).
44. Barba-Bon, A., Costero, A. M., Gil, S., Harriman, A. & Sancenón, F. Highly selective detection of nerve agent simulants with BODIPY dyes. *Chem. Eur. J.* **20**, 6339–6347 (2014).
45. Houten, K. A. V., Heath, D. C. & Pilato, R. S. Rapid Luminescent detection of phosphate esters in solution and the gas phase using (dppe)Pt(S₂C₂(2-pyridyl)(CH₂CH₂OH)). *J. Am. Chem. Soc.* **120**, 12359–12360 (1998).
46. Zhang, S.-W. & Swager, T. M. Fluorescent detection of chemical warfare agents: functional group specific ratiometric chemosensors. *J. Am. Chem. Soc.* **125**, 3420–3421 (2003).
47. Dale, T. J. & Rebek, J. Jr. Fluorescent sensors for organophosphorus nerve agent mimics. *J. Am. Chem. Soc.* **128**, 4500–4501 (2006).
48. Gupta, M. & Lee, H. A pyrene derived CO₂-responsive polymeric probe for the turn-on fluorescent detection of nerve agent mimics with tunable sensitivity. *Macromolecules* **50**, 6888–6895 (2017).
49. Jang, Y. J., Mulay, S. V., Kim, Y., Jorayev, P. & Churchill, D. G. Nerve agent simulant diethyl chlorophosphate detection using a cyclization reaction approach with high stokes shift system. *N. J. Chem.* **41**, 1653–1658 (2017).
50. Gotor, R. et al. BODIPY dyes functionalized with 2-(2-dimethylaminophenyl)ethanol moieties as selective OFF-ON fluorescent chemodosimeters for the nerve agent mimics DCNP and DFP. *RSC Adv.* **4**, 15975–15982 (2014).
51. Climent, E. et al. Determination of the chemical warfare agents Sarin, Soman and Tabun in natural waters employing fluorescent hybrid silica materials. *Sens. Actuat B-Chem.* **246**, 1056–1065 (2017).
52. Dennison, G. H. & Johnston, M. R. Mechanistic insights into the luminescent sensing of organophosphorus chemical warfare agents and simulants using trivalent lanthanide complexes. *Chem. Eur. J.* **21**, 6328–6338 (2015).
53. Dennison, G. H. et al. Qualitative colorimetric analysis of a Ir(III)/Eu(III) dyad in the presence of chemical warfare agents and simulants on a paper matrix. *RSC Adv.* **9**, 7615–7619 (2019).
54. Metherell, A. J. et al. Converting an intensity-based sensor to a ratiometric sensor: luminescence colour switching of an Ir/Eu dyad upon binding of a V-series chemical warfare agent simulant. *J. Mater. Chem. C* **4**, 9664–9668 (2016).
55. Knapton, D., Burnworth, M., Rowan, S. J. & Weder, C. Fluorescent organometallic sensors for the detection of chemical-warfare-agent mimics. *Angew. Chem. Int. Ed.* **45**, 5825–5829 (2006).
56. Royo, S. et al. Chromogenic, specific detection of the nerve-agent mimic DCNP (a Tabun Mimic). *Chem. Eur. J.* **17**, 6931–6934 (2011).
57. Rosenblatt, D. H., Small, M. J., Kimmell, T. A. & Anderson, A. W. *Background Chemistry for chemical warfare agents and decontamination processes in support of delisting waste streams at the U.S. Army Dugway Proving Ground, Utah*, pp. 8–35 (OSTI, TN, USA, 1996).
58. Franca, T. C. C. et al. Novichoks: the dangerous fourth generation of chemical weapons. *Int. J. Mol. Sci.* **20**, 1222 (2019).
59. Gao, J. et al. Diisopropylfluorophosphate impairs the transport of membrane-bound organelles in rat cortical axons. *J. Pharmacol. Exp. Ther.* **356**, 645–655 (2016).

60. Alam, T. M., Kinnan, M. K., Wilson, B. W. & Wheeler, D. R. Sub-equimolar hydrolysis and condensation of organophosphates. *ChemistrySelect* **1**, 2698–2705 (2016).
61. Heiss, D. R. et al. Synthesis and storage stability of diisopropylfluorophosphate. *J. Chem.* **2016**, 3190891 (2016).
62. Ward, J. R., Hovanec, J. W., Albizo, J. M., Szafraniec, L. L. & Beaudry, W. T. Decomposition of phosphonofluoridates on glass. *J. Fluor. Chem.* **51**, 277–282 (1991).
63. Purohit, A. K. et al. A single-step one pot synthesis of dialkyl fluorophosphates from dialkylphosphites. *Tetrahedron Lett.* **56**, 4593–4595 (2015).
64. Perumgani, P. C., Kodicherla, B., Mandapati, M. R. & Parvathaneni, S. P. Suzuki-Miyaura cross-coupling for efficient synthesis of aryl-substituted N-heteroarenes catalyzed by recyclable N-phenylpiperazine-Palladium(II) complex. *Inorg. Chim. Acta* **477**, 227–232 (2018).
65. Thomas, K. R. J. et al. Efficient red-emitting cyclometalated iridium(III) complexes containing lepidine-based ligands. *Inorg. Chem.* **44**, 5677–5685 (2005).
66. Nilsson, J., Kraszewski, A. & Stawinski, J. Reinvestigation of the ³¹P NMR evidence for the formation of diorganyl phosphoropyridinium intermediates. *J. Chem. Soc. Perkin Trans. 2*, 2263–2266 (2001).

Acknowledgements

P.E.S. is supported by The University of Queensland Amplify Initiative. P.L.B. is an Australian Research Council Laureate Fellow (FL160100067). This research was supported by funding from the Australian Research Council under the Discovery Program (DP170102072). We thank Dr. Kylie Vongsanga, Mr Orazio Campanale, Ms Eva Micich, Mr Claudio Ceccato for assistance in the measurements using Sarin. The provision of financial or research support does not constitute an express or implied endorsement of the results or conclusions presented here by DST Group or the Australian Department of Defence.

Author contributions

S.F. synthesized and characterized the sensing compounds and undertook the sensing measurements and analysis with the chemical warfare agent simulants under the

guidance of P.L.B., P.E.S., and I.R.G.. G.H.D. and N.F. were responsible for organizing the sensing measurements using Sarin. P.L.B. initiated the chemical warfare agent detection program. All authors contributed to the interpretation of the results and preparation of manuscript. All authors have given approval to the final version of the manuscript.

Competing interests

The authors declare no competing interests.

Additional information

Supplementary information The online version contains supplementary material available at <https://doi.org/10.1038/s42004-021-00482-6>.

Correspondence and requests for materials should be addressed to P.L.B. or P.E.S.

Reprints and permission information is available at <http://www.nature.com/reprints>

Publisher's note Springer Nature remains neutral with regard to jurisdictional claims in published maps and institutional affiliations.



Open Access This article is licensed under a Creative Commons Attribution 4.0 International License, which permits use, sharing, adaptation, distribution and reproduction in any medium or format, as long as you give appropriate credit to the original author(s) and the source, provide a link to the Creative Commons license, and indicate if changes were made. The images or other third party material in this article are included in the article's Creative Commons license, unless indicated otherwise in a credit line to the material. If material is not included in the article's Creative Commons license and your intended use is not permitted by statutory regulation or exceeds the permitted use, you will need to obtain permission directly from the copyright holder. To view a copy of this license, visit <http://creativecommons.org/licenses/by/4.0/>.

© The Author(s) 2021